BLOCKY CRATERS: IMPLICATIONS ABOUT THE LUNAR MEGAREGOLITH*

T. W. THOMPSON, W. J. ROBERTS, and W. K. HARTMANN
Planetary Science Institute, Pasadena, Calif.; and Tucson, Arizona, U.S.A.

R. W. SHORTHILL
University of Utah Research Institute, Salt Lake City, Utah, U.S.A.

and

S. H. ZISK
NEROC Haystack Observatory, Westford, Mass., U.S.A.

(Received 9 May, 1979)

Abstract. Radar, infrared, and photogeologic properties of lunar craters have been studied to determine whether there is a systematic difference in blocky craters between the maria and terrae and whether this difference may be due to a deep megaregolith of pulverized material forming the terra surface, as opposed to a layer of semi-coherent basalt flows forming the mare surface. Some 1310 craters from about 4 to 100 km diameter have been catalogued as radar and/or infrared anomalies. In addition, a study of Apollo Orbital Photography confirmed that the radar and infrared anomalies are correlated with blocky rubble around the crater.

Analysis of the radar and infrared data indicated systematic terra–mare differences. Fresh terra craters smaller than 12 km were less likely to be infrared and radar anomalies than comparable mare craters: but terra and mare craters larger than 12 km had similar infrared and radar signatures. Also, there are many terra craters which are radar bright but not infrared anomalies.

Our interpretation of these data is that while the maria are rock layers (basaltic flow units) where craters eject boulder fields, the terrae are covered by relatively pulverized megaregolith at least 2 km deep, where craters eject less rocky rubble. Blocky rubble, either in the form of actual rocks or partly consolidated blocks, contributes to the radar and infrared signatures of the crater. However, aging by impacts rapidly destroys these effects, possibly through burial by secondary debris or by disintegration of the blocks themselves, especially in terra regions.

1. Introduction

Current models for the Moon's evolution hypothesize the following sequence of events:

(1) Formation of a crust at 4.6 aeons ago followed by an intense period of bombardment until about 3.7 aeons ago.

(2) Formation of mare surfaces and continued bombardment at a lower level from 3.7 to 3.2 aeons ago.

(3) Continued lesser bombardment with smaller bodies to the present time.

Thus, the lunar highlands (the terrae) should be covered with a megaregolith, a fragmental debris which is kilometers thick and the lunar maria should be coherent or partially fractured rock slabs which are kilometers thick.

* PSI Contribution No. 110.

The Moon and the Planets **21** (1979) 319–342. 0165–0807/79/0213–0319$03.60.

The thickness of both the megaregolith debris layers and mare rock layers are key elements in our study. Megaregolith thickness was estimated to be about 2 km by Hartmann (1973) who proposed that intense early cratering destroyed rocks older than 4.1 aeons in the upper part of the megaregolith. Short and Forman (1972), computing volumes of crater ejecta from existing terra craters, predict terra megaregolith depths of 1.4 to 2.4 km. Monte Carlo computer simulations of terra impacts predicts that 50% of the highlands is cratered to 2–3 km (Hörz *et al.*, 1967). Also, Short and Forman (1972), McGetchin *et al.* (1973) and Moore *et al.* (1974), have shown that basin impacts will add eject blankets to the terra with depths of few tens of meters to a few kilometers. In addition, analysis of seismic profiles by Kovack and Watkins (1973) indicate that "from about 4 km to 25 km depth the physical properties of lunar rocks are probably dominated by cracks, pores and inter-granular effects".

The rock layers of mare basalts in the irregular (shallow) maria probably range from 0.5 to 1.5 km, based on DeHon's studies (1973, 1978) of ghost craters in Maria Nectaris, Tranquillitatus, Nubium, and Humorum. Deep, basin mare basalts may range from 1.0 to 4.0 km deep. For example, gravity modeling of the Mare Serenitatis mascon indicates mare depths of at least 3 km, (Phillips *et al.*, 1972). The Apollo Lunar Sounder mapped subsurface radar echoes on Mare Crisium and Mare Serenitatis from depths of 0.9 to 1.6 km (Peeples *et al.*, 1978). The maria are now covered with a thin (3 to 10 m deep) regolith (see Shoemaker *et al.*, 1970).

If the maria are layers of solid or partially fractured rock and the terrae are layers of pulverized fragmental debris, then impacts into these layers should create different types of craters in these two types of terrain. Even if the terra megaregolith were purely fine dust, impacts might create shock-lithified meter-sized blocks. It is more likely that the megaregolith contains many meter sized rocks, which have experienced many impacts and which are exposed by impacts. However, mare crater ejecta derived from coherent or partially fractured rock layers should contain more solid rocks. Also, these mare crater ejecta should survive longer than terra crater ejecta when these craters are subjected to aging from meteoritic bombardment. Thus, we expect smaller mare craters to be blockier than terra craters of the same size.

There is some evidence already for mare–terra differences in blocky craters. For example, Apollo 16 samples from the Descartes Highlands landing site were mostly breccias, while samples from the other mare landing sites were mostly coherent rock fragments. Also, Ronca (1970) has shown that infrared anomalies, craters with excess surface rocks, are more likely to occur in the mare than in the terra. To search further for mare–terra differences in blocky craters, infrared and radar anomalies will be used to indicate blocky craters. Thompson *et al.* (1974), found that the likely source of these infrared and radar anomalies was excess surface and/or subsurface rocks in crater ejecta by correlating infrared and radar anomalies associated with 51 lunar craters using 10 μm infrared, 3.8 cm, and 70 cm radar maps of the Moon.

The work reported here will expand upon the earlier study of Thompson *et al.* (1974). In particular, a catalog of 1310 infrared and radar anomalies was created from the 10 μm

infrared, 3.8 cm, and 70 cm radar maps. Statistical studies of this catalog provided a better understanding of the occurrence of different anomaly combinations. Size-frequency distributions of different crater types indicated variations between the maria and terra for different sized craters. In addition, Apollo orbital photography was also studied in order to relate infrared and radar signatures to surface block and ages of craters.

These investigations were designed to further clarify the physical nature of radar/infrared anomalies and provide insights into the character and rate of lunar surface processes. In this paper, our attention was focused on the thickness of the fragmental layer covering the lunar terra using size–frequency distributions of anomaly type as a means of probing the properties of the Moon to different depths.

2. Crater Related Radar and Infrared Anomalies on the Moon

In order to provide a background for the remainder of this report, it is useful to review the earlier work of Thompson *et al.* (1974) and to comment briefly on our study of Apollo Orbital Photography. The former provides a basis for implying surface and subsurface rock distributions from radar and infrared signatures; the later establishes that craters with the large blocky rubble that can be detected from orbit are strong radar and infrared anomalies. Our study of Apollo Orbital Photography is given in Appendix A.

The earlier work of Thompson *et al.* (1974) provides a background for describing surface and subsurface rock distributions from the various combinations of infrared and radar anomalies as shown in Table I. Briefly, an infrared anomaly is a localized area that remains warmer than its environs during a lunar eclipse. The likely source of infrared anomalies are excess numbers of bare surface rocks which are greater than 10 cm in size and reradiate stored heat during a lunar eclipse. Radar anomalies are localized areas which appear to backscatter more power than their environs after removal of slope effects. The likely source for radar anomalies are excess number of rocks which have sizes between one-quarter and ten radar wavelengths. These rocks could be on the surface or buried no deeper than about 30 radar wavelengths. Thus, the 3.8 cm radar echo-power is controlled by rocks with sizes between 1 cm and 40 cm and on the surface or buried no deeper than 1.2 m; the 70 cm radar echo-power is controlled by rocks which are between 20 cm and 7.0 m and on the surface or buried no deeper than 20 m. The interpretation of the various combinations of infrared and radar anomalies as it relates the physical properties to crater ejecta is given later in this report.

In addition, our study of Apollo Orbital Photography which is given in Appendix A established that young craters with large blocks in their ejecta have strong radar and infrared anomalies. This is illustrated in Figure 1 which shows the boulder and pit density of nineteen smaller craters. Younger craters, those with more boulders and fewer pits, tend to be infrared and radar anomalies; older craters with fewer boulders and more pits tend to have average infrared and radar signatures.

Given that infrared and radar anomalies can be related to crater ejecta with excess numbers of surface and subsurface rocks, then the hypothesized mare–terra difference in

TABLE I

Surface conditions implied by various combinations or infrared and radar anomalies

ANOMALY INDEX (IR-3.8cm-70cm)	IMPLIED SURFACE CONDITIONS
B--	Excess surface rocks with sizes larger than 10cm.
-B-	Excess rocks with sizes of 1 to 40cm on the surface or buried no deeper than 1.2 meters.
--B	Excess rocks with sizes of 20cm to 7.0cm on the surface or buried no deeper than 20 meters.
BBB	Excess surface rocks with sizes of 1cm to 7.0 meters.
FBB	Average population of surface rocks with sizes greater than 10cm. Excess buried rocks with sizes of 1 to 40 centimeters within 1.2m of surface. Excess buried rocks with sizes of 20cm to 7.0 meters within 20m of surface.
FBF	Average surface rocks with sizes 10cm and greater. Excess buried and surface rocks with sizes 1-40cm. Average buried rocks with sizes of 20cm to 70m within 20m of surface.
FFB	Average surface rocks with sizes 1cm and greater. Average buried rocks with sizes 1-40cm within 1.2cm of surface. Excess buried rocks with sizes 1cm-7.0m within 20m of surface.
BBF	Excess surface rocks with sizes 1cm to 20cm. Average surface rocks with sizes 20cm to 7.0m. Average buried rocks with sizes 20cm to 7.0 meters within 20m of surface.
BFB	Excess surface rocks with sizes 40cm to 7.0m. Average surface rocks with sizes 1-40cm.
BFF	Excess surface rocks with sizes 7.0 meters and larger. Average surface rocks with sizes 1cm-7.0 meters.
FFF	Average surface, no excess surface and subsurface rocks.

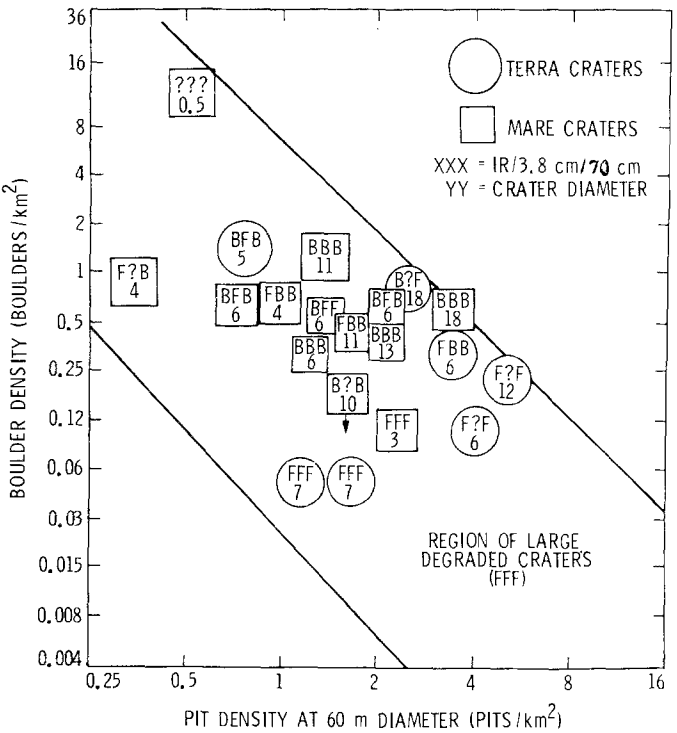

Fig. 1. Boulder and pit density for eighteen small craters which were studied in detail as described in Appendix A. Younger craters, those with fewer pits and more boulders tend to be strong infrared an radar anomalies; older craters with more pits and fewer boulders tend to have average infrared and radar responses. Table I describes the three-letter infrared-radar index.

the blocky craters should appear in statistics of infrared and radar anomaly occurrence. To test this, a catalog of infrared and radar anomalies was derived from existing infrared and radar maps of the Moon. The infrared data were originally taken during the lunar eclipse of 19 December 1964 using the Kottamia telescope of the Helwan Observatory, Egypt (Shorthill, 1973). The 3.8 cm radar data were obtained in a series of observations from 1966 to 1970 using the 7940 MHz radar at the M.I.T. Haystack Observatory (Zisk *et al.*, 1974). The 70 cm radar data were obtained between 1966 and 1969 using the 430 MHz radar at the Arecibo Observatory, Puerto Rico (Thompson, 1974). Surface resolution for these observations was 1–3 km for the 3.8 cm radar, 5–10 km for the 70 cm radar, and 14–30 km for the infrared observations.

The catalog derived drom the infrared and radar data contained 1310 craters. Craters on the limb beyond the area of the available LAC charts were ignored. There is no 70 cm radar data for these areas and the infrared resolution is poor. This crater catalog covered about one-half of the Earth-visible surface. Craters were identified with number of quantities to indicate their environs (mare or terra), size, and position. Mare–terra background indicators were determined from USGS Lunar Geological Maps. All mare

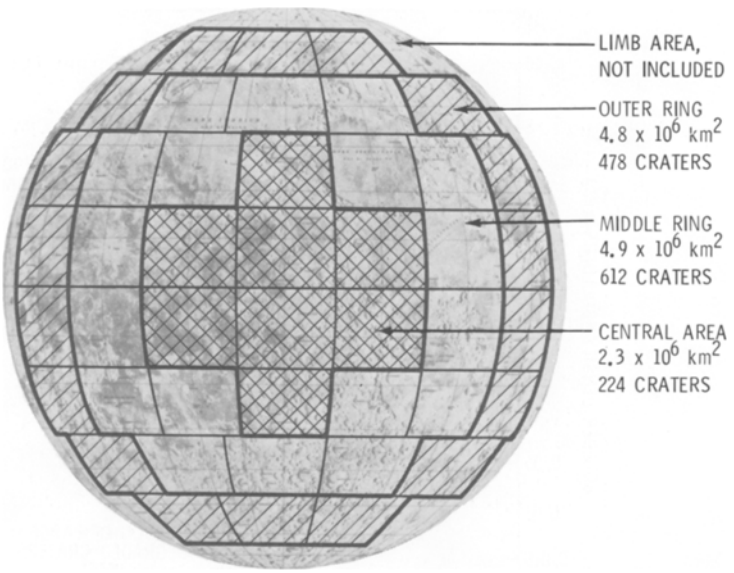

Fig. 2. Central area, Middle and Outer Rings used for the statistical study of infrared and radar anomalies. No craters were cataloged for limb areas beyond the areas covered by the availabe LAC chart.

craters were lumped together whether they were in the irregular or circular (basin) maria. All terra craters were lumped together whether they were near or far from basins. Crater names, positions, and diameters were taken from the Lunar and Planetary Laboratory (LPL) catalogs (Arthur *et al.*, 1963, 1964, 1965 and 1966).

In order to simplify the statistical analysis of these radar and infrared anomalies, signal strengths were ignored and the craters were either anomalous or average. A radar anomaly had to backscatter twice or more power than its environs. This simplification of assigning radar and infrared anomalies as only anomalous or average is reasonable since it is difficult to properly model ejecta and rim effects for smaller craters. Many of the craters in our catalog are covered by only a few resolution cells. Often signals come from the ejecta blanket beyond the rim and crater rims can modulate signals for the simple reason that they are tilted. Modeling of these rim and ejecta effects is difficult and beyond the scope of this research.

Since the infrared and radar signatures was characterized by binary choice, the infrared and radar signals for a crater are given by a three letter code, *XYZ*. *X* takes the value B (bright) where there is an infrared anomaly and F (faint) for no anomaly, *Y* and *Z* were similarily assigned based on the 3.8 cm and 70 cm radar signals. There are eight possible anomaly types.

The crater data given in the catalog is subject to a number of systematic errors which are not related to crater blockiness. As described in Appendix B, the 70 cm radar and infrared resolutions are relatively coarse permitting some small craters to be misidentified as being average when they should have appeared as anomalies. The infrared resolution varies from the center to the limb so this loss of infrared signatures may be worse toward

Table II

	CENTRAL+ AREA	MIDDLE+ RING	OUTER+ RING
BFF* ANOMALIES / 10^6 km^2	7.8	2.0	2.5
BBF* ANOMALIES / 10^6 km^2	9.1	4.9	3.3
BFB* ANOMALIES / 10^6 km^2	2.2	1.8	1.9
FBB* ANOMALIES / 10^6 km^2	16.5	31.4	22.9
FFB* ANOMALIES / 10^6 km^2	3.5	8.1	11.7
FBF* ANOMALIES / 10^6 km^2	16.1	32.0	27.0
BBB* ANOMALIES / 10^6 km^2	30.0	40.2	29.6
TOTAL NUMBER OF ANOMALIES / 10^6 km^2	85.2	120.4	94.8
MARE AREA (10^6 km^2)	1.0	2.7	1.7
TERRA AREA (10^6 km^2)	1.3	2.2	3.1
TOTAL AREA (10^6 km^2)	2.3	4.9	4.8

* IR/3.8 cm RADAR /70 cm RADAR INDEX
\+ SEE FIGURE 2

the limb. Also, the radar esponse from crater rims may also provide false signals toward the limb.

To search for these systematic geometry effects and the hypothesized mare–terra difference in blocky craters, the statistics for all anomaly types were generated for three independent areas – the Central Area, Middle and Outer Ring Areas shown in Figure 2. These three areas have nearly equal mare, terra and total areas as shown in Table II.

This division into three areas coupled with the eight possible anomaly combinations generated some twenty-four cases to consider. Fortunately, a number of these combinations can be eliminated by two simple criteria. First, the anomaly type (FFF) was not considered and three anomaly types (BFF, BFB, and BBF types) were eliminated since they were uncommon and their distributions had large statistical errors. Second, the Central Area was eliminated since its crater distributions were significantly different from the Middle and Outer Rings. Because of poor radar data for areas near the center of the disk, the rare (BFF, BFB, and BBF) anomalies in the Central Area occur twice as frequently as in the Middle and Outer Rings while the common (FBB, FBF, FFB, and BBB) anomalies occur half as frequently as shown in Table II.

This first level of selection reduced the number of crater-size distributions to eight cases – BBB, FBB, FBF and FFB anomaly types for the Middle and Outer Ring areas. The BBB, FBB, and FBF anomaly types had similar distributions for the Middle and Outer Rings, so crater statistics were combined and a single plot was generated for the combined Middle and Outer Rings as shown in Figures 3 and 4. For the FFB anomaly type, the Middle and Outer Ring are given as separate plotes in Figure 5.

The occurence of infrared and radar anomalies is illustrated here in Figures 3, 4 and 5

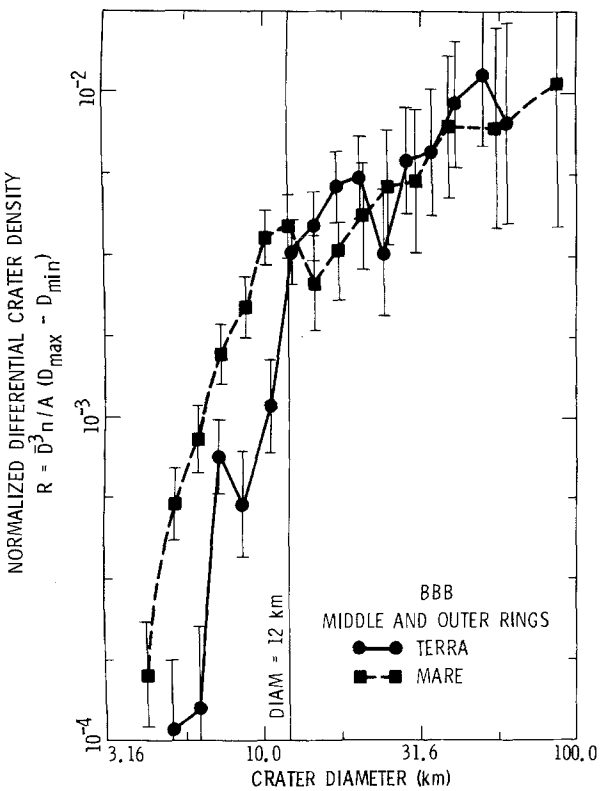

Fig. 3. Differential distributions for mare and terra BBB (bright IR, bright 70 cm and 3.8 cm radar) craters in the Middle and Outer Ring areas shown in Figure 2.

using differential distributions following the recommendations of Woronow *et al.* (1978). These differential distributions are plotted as R versus crater diameter; the quantity R is $(\bar{D})^3 N/A(D_{\max} - D_{\min})$ where $\bar{D}$ is the geometric mean of crater diameters, N is the number of craters. A is the area, and $D_{\max}$, $D_{\min}$ are the maximum and minmum crater diameters for each diameter size bin. Woronow *et al.* (1978) shows that differential distribution proportional to (crater diameter)$^{-3}$ plots is a horizontal line in a R versus diameter plot.

3. Mare–Terra Differences in Radar/Infrared Anomalies

Significant systematic differences between mare and terra appear in the statistics of infrared and radar anomaly occurence which are illustrated in Figures 3 through 5. For example, the densities of BBB (bright at all wavelengths) craters is comparible on the maria and terra for craters with diameters larger than 12 km while mare BBB type craters occur 3 to 5 times more frequently than terra BBB type craters when crater diameter is less than 12 km. This difference in BBB type craters is illustrated further in Figure 6 which

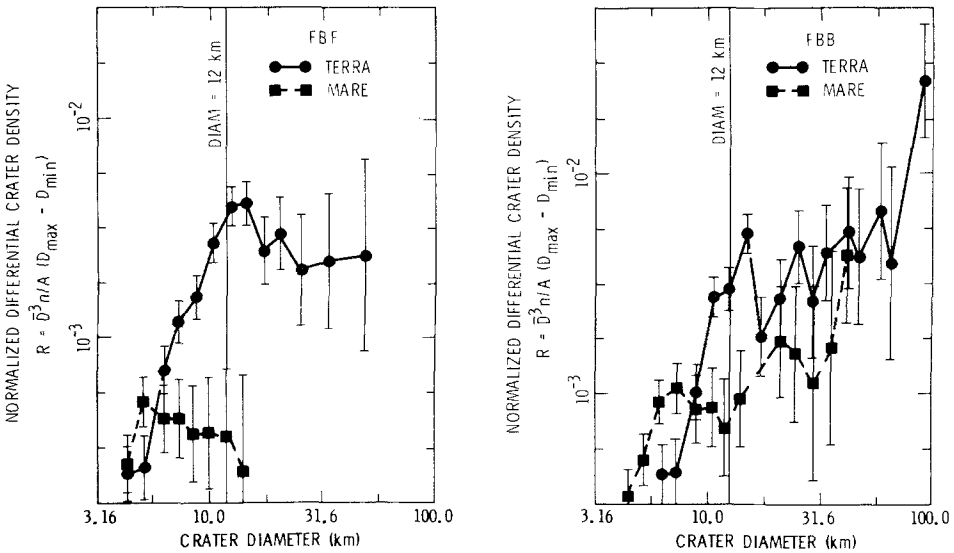

Fig. 4. Differential distributions for mare and terra FBB (faint IR, bright 3.8 cm and 70 cm radar) and FBF (faint IR, bright 3.8 cm radar and faint 70 cm radar) craters in the Middle and Outer Ring Areas shown in Figure 2.

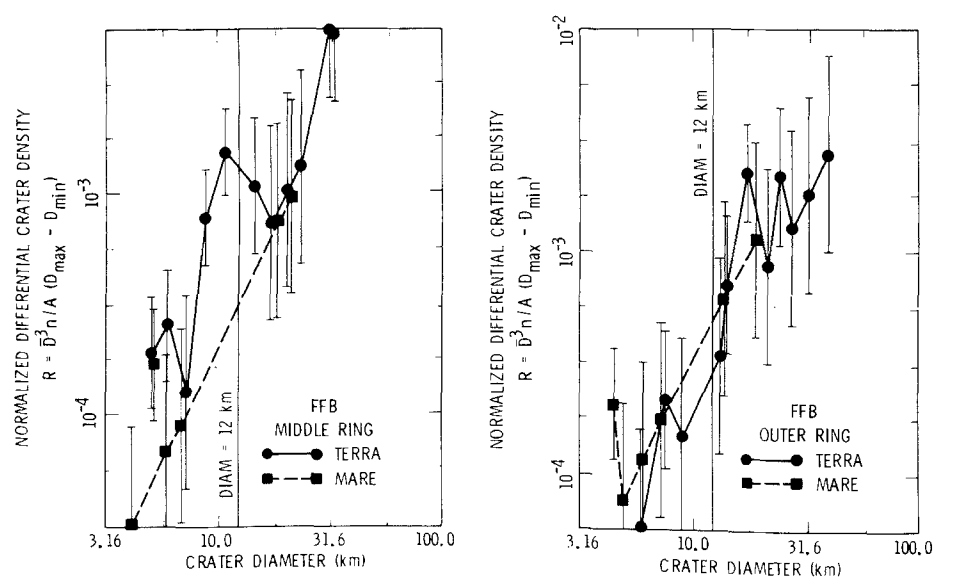

Fig. 5. Differential distribution for mare and terra FFB (faint IR, and 3.8 cm radar, bright 70 cm radar) craters for the Middle Ring and Outer Ring areas shown in Figure 2.

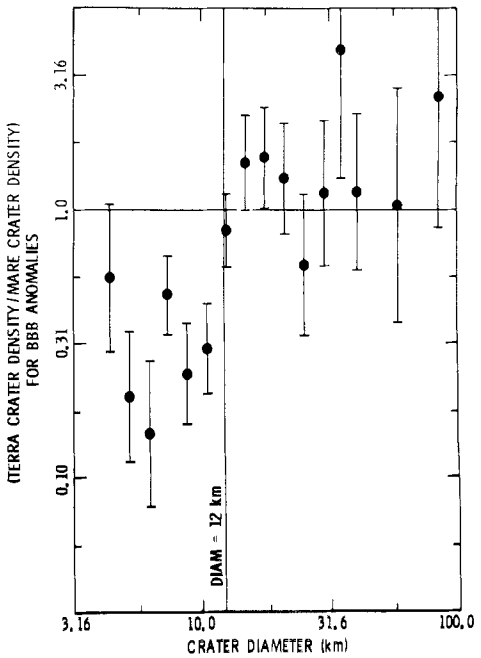

Fig. 6. Distributions of terra BBB anomalies relative to mare BBB craters for the Middle and Outer Ring areas shown in Figure 2.

shows the ratio of terra to mare crater differential distributions plotted versus crater diameter.

The other common anomalies – the FBB, FFB and FBF anomalies – have mare–terra differences which are different than the mare–terra difference associated with the BBB type crater. The FBB, FFB and FBF type anomalies (craters with average infrared signals and radar anomalies) occur frequently in the terra, and infrequently in the mare. Furthermore, terra densities are low for smaller craters and rise sharply when crater diameters increases from 5 to 15 km.

In order to interpret the mare–terra differences in infrared and radar anomaly occurence illustrated in Table II and Figures 3 through 6, it is useful to review Table I, which gives the implications about surface and subsurface rocks that can be made from various combinations of anomalies. First, consider a crater which is a BBB (bright at all wavelengths) anomaly. Here, the infrared and radar behaviors imply excess surface rocks of sizes from one centimeter to 7.0 cm. Thus, the BBB anomaly is a direct indicator of a blocky crater, the prime subject of this study.

As a second step, consider the three anomaly types which are fiant in the infrared maps and bright in the one or both radar maps. Since radar waves can penetrate into the surface and detect buried rocks, these anomalies imply craters with average surface rock

populations with excess buried rocks. For example, the FBB (faint infrared, bright 3.8 cm and 70 cm radar) implies excess buried rocks with sizes of 1 to 20 cm within 1.2 m of the surface and excess buried rocks with sizes of 20 cm to 7.0 m buried within 20 m of the surface. Similarly, the FBF (faint infrared, bright 3.8 cm radar, faint 70 cm radar) anomaly implies only excess centimeter sized rocks within 1 m of the surface and the FFB (faint infrared and 3.8 cm radar, bright 70 cm radar) anomaly implies only excess meter rocks with deeper burials.

As the third step, consider the three anomaly types which are bright in the infrared and faint in one or both radar wavelengths. The bright infrared response implies excess surface rocks and the radar responses imply rock sizes. For example, a BBF (bright infrared and 3.8 cm radar, faint 70 cm radar) anomaly implies excess surface rocks with sizes of 1 to 20 cm and average rock populations for meter sized rocks. Similarly, the BFB (bright infrared, faint 3.8 cm radar and bright 70 cm radar) anomaly implies excess surface rocks with sizes greater than 40 cm and the BFF (bright infrared, faint 3.8 cm and 70 cm radar) anomaly implies excess surface rocks with sizes greater than 20 m. Last, the FFF (faint at all wavelengths) anomaly implies average surface and subsurface rock populations.

These interpretations of infrared and radar anomalies are collabroated by the photogeologic study of Apollo Orbital Photography which is detailed in Appendix A and illustrated in Figure 1. Note that Figure 1 shows the craters with infrared and radar anomalies have high boulder densities while the FFF (faint at all wavelengths) type craters have low boulder densities.

4. Megaregolith Properties from Mare–Terra Differences in Infrared Radar Anomaly Occurrence

The more common infrared and radar anomalies show significant systematic differences between maria and terra. Let us now consider how different properties of the megaregolith can be determined from the crater distributions shown in Figures 3 through 6.

Perhaps the most significant plots are Figures 3 and 6, which show the distributions of BBB type craters. These craters, which are bright at all three wavelengths, are the best indicators of blocky craters. The differential distributions for these craters shows that blocky craters with diameters greater than 12.0 km are equally likely to occur in the mare and terra, while for blocky craters with diameters less than 12.0 km, mare craters are more numerous. This suggests that terra craters with diameters on the order of 12 km result from craters which just pierce the megaregolith. The ejecta for smaller terra craters contains previously fractured and brecciated rocks from the megaregolith, while the ejecta for large terra craters contains more cohesive rocks from layers underneath the megaregolith. According to the formula derived by Pike (1977), young lunar craters with diameters of 12.0 km have a depth of 2.0 km below the preimpact surface. This depth of 2.0 km is our estimate for the depth of the megaregolith.

In addition to the BBB type craters, the other common anomaly types provides additional implications about the lunar megaregolith. Table II shows that the BBB type

Table III
IR/radar anomaly statistics (diameter > 10 km)

ANOMALY TYPE (IR/3.8 cm/70 cm) DIAM. ≥ 10 km	MARE CRATERS PER 10^6 km^2	TERRA CRATERS PER 10^6 km^2	PERCENTAGE LPL AGE CLASS 1 (YOUNGEST)	PERCENTAGE LPL AGE CLASS 2	PERCENTAGE LPL AGE CLASS 3 (MIDDLE AGE)
BBB	18.1	20.1	70%	27%	3%
FBB	5.0	18.1	72%	27%	1%
FBF	0.9	19.5	64%	35%	1%
FFB	0.9	6.1	14%	62%	24%
	MARE AREA — 4.4×10^6 km^2	TERRA AREA — 5.4×10^6 km^2			

crater is the most common anomaly, the FBB, FBF, and FFB type craters are common and the BFF, BFB and BBF type craters are rare. These rare craters are infrared anomalies where one or both radars are average; these craters would have excess surface rocks with specific sizes. In contrast, the common anomalies are radar anomalies with an average infrared response; these craters would have average populations of surface rocks with excess subsurface rocks of centimeter and/or meter size. Also, the crater size–frequency distributions of Figures 4 and 5 show that the larger faint infrared-bright radar craters occur more frequently in the terra than in the mare.

All of these data imply that the aging of impact craters first drives surface rocks to normal densities and then later drives subsurface rock populations in the first few meters to normal densities. Furthermore, it seems likely that the larger terra BBB type craters are post-mare in age while the average infrared–radar bright craters are pre-mare in age. This is not surprising since mare regolith depths are between 3 and 10 m (Shoemaker *et al.* 1970). A terra crater formed after mare emplacement would be gardened to similar depths. The meteoritic bombardment which produced 3 to 10 m of regolith still excavated enough underlying rubble to create excess surface and subsurface polulations of meter and centimeter sized rocks. The surfaces of older, larger terra craters have been gardened to deeper depths, leaving average surface rock populations and some excess subsurface rocks. This, in general, agrees with rock like time computed by Shoemaker *et al.* (1970), and the age classes assigned by Arthur *et al.* (1963, 1964, 1965, 1966) as shown in Table III.

The differential distributions for the common craters which are radar anomalies with average infrared responses show markedly differences between smaller and larger craters. Figures 4 and 5 show that the relative numbers of these types of terra craters rise sharply

when crater diameters increase from 5 to 15 km. Also, for the smaller FBB and FFB type anomalies, there are more mare craters than terra craters. This is consistent with the hypothesis that the ejecta from smaller terra craters is fragmental debris which breakup under meteoritic impact and gardening while ejecta from smaller mare craters is coherent rock weather meteoritic impacts for longer times.

In addition to providing information about the megaregolith, the size-frequency distribution of the common FBB, FBF and FFB anomalies may provide an estimate of larger lunar impacts between Oriental basin formation and mare formation. The discussion above implies that gardening by meteorites and smaller cratering events will eventually erase all excess populations of surface and subsurface rocks. This gardening was possibly interrupted by the Orientale event, since Moore *et al.* (1974) show that Oriental ejecta could have covered all of the Moon with depths of 20 m or more. Existing blocky craters at that time would have ben covered with enough ejecta to erase their populations of excess surface and subsurface rocks. Larger craters formed since the Orientale event would be first blocky and then subjected to meteoritic bombardment. Larger terra craters formed since mare formation would still be the BBB type (bright at all wavelengths anomaly), while craters formed between the Orientale event and mare formation would be gardened to the point where there were excess surface rocks, but some excess numbers of subsurface rocks still remain. Thus, craters formed in this intervening time period would be radar anomalies with average infrared responses – FBB, FBF, and FFB anomalies.

5. Summary

Both the statistical study of infrared and radar anomalies and the photogeologic study of Apollo Orbital Photography (Appendix A) support the contention that the terra has a megaregolith of comminuted material that is considerably deeper than the regolith of the maria. The depth of megaregolith is 2.0 km based on Pike's depth-to-diameter data and our observation that terra craters become blocky at 12.0 km diameter. Also, our photographic and statistical study indicate that terra ejecta is relatively block free. We cannot tell whether this is due to having fewer rocks in the ejecta originally, to having ejecta that is primarily friable breccias, or to both effects.

Our estimate of 2.0 km for the megaregolith depth agrees with previous estimates of Hartmann (1973), Short and Forman (1972), Hörz *et al.* (1976), and Aggarwal and Oberbeck (1979). However, our results are not consistent with the alternate hypothesis by Gold (1977) that the maria are vast dust basins formed by stripping dust off the lunar highlands. This hypothesis would predict that smaller terra craters would be blockier than smaller mare craters, while the opposite effect is actually observed. Also, the high density of pores and fractures to depths of 25 km implied by interpretation of lunar seismic profiles (Kovach and Watkins, 1973) seem to have little effect on controlling the blockiness of crater ejecta.

Our estimate of a depth of 2.0 km for a pulverized layer of megaregolith in the terrae leads to the question of significance of this figure, in terms of lunar surface evolution. For

example, since this is comparable to the depth of the larger craters that saturate or nearly saturate the uplands, does it mean that the total upland cratering has only once-saturated the uplands since the terra crust formed, rather than saturating the surface many times over the craters? We find it difficult to address this question for two reasons. First, the pulverized layer may or may not grade continuously into layers with layer fragments and deeper layers that are mearly heavily fractured. Or, it might be bounded sharply by a deep surface below which thermal metamorphism has bounded the megaregolith fragments into strong breccias. The craters, which are used to make the measurement, also grade from a pulverized zone to a fractured zone in their subsurface structure. Thus, without a clearer understanding of the megaregolith subsurface structure and the effects of craters in it, it is hard to infer structural or historical meaning from the finding that craters shallower than 2.0 km throw out fewer boulders than deeper craters. Secondly, we are unaware of reliable models of how the megaregolith depth evolves with increased crater density. For example, if cratering just to the saturation point by N craters creates a megaregolith of depth D, would $2N$ craters make a regolith of depth $2D$? Probably not, since doubling the number of the craters increases the size of the largest crater (in a -2 power law cumulative size distribution) by only 1.4 times, not 2 times. The megaregolith may thus not migrate downward linearly with increasing numbers of craters, especially once saturation has been approached.

For these reasons, we conclude only that the upper 2.0 km of terra crust are relatively pulverized, but do not draw a conclusion on the amount of cratering necessary to do this, or on whether the bottom of this layer is bounded sharp (such as by metamorphosed coherent braccias) or gradual (such as by increasing numbers of large coherent fragments).

Further work based on this successful identification of mare and terra differences is suggested. Both the infrared and 70 cm radar data could be improved with new observations and better resolution with other remote sensing techniques such as optical spectrography may help identify blocky craters. Also, blocky crater distributions should be studied for areas selected using other criteria. For example, do the irregular and basin maria have different distributions? Do the terra areas with expected thick deposits of basin ejecta have different distributions of blocky craters? Do blocky crater distribution provide insights into the Moon-wide distribution of ejecta from Mare Orientale? In addition, Venusian regolith depths may be determined using radar reflectance to identify blocky craters if an orbiting radar is flown to Venus.

Acknowledgements

Funding for this study was provided by NASA Grant NASW-3117. The interpretation of Apollo Orbital Photographs was done at the Space Photographic Libraries at the Lunar and Planetary Institute, Clear Lake City, Texas and at the Lunar and Planetary Laboratory, University of Arizona, Tucson, Arizona. The cataloging of infrared and radar anomalies made extensive use of map displays generated by Apollo Experiment S-217.

Appendix A. A Photogeologic Study of Blocky Craters

The hypothesis that mare and terra craters have different rock distributions was checked directly with high resolution Apollo Orbital photography. Since other portions of this report will study mare–terra differences in infrared and radar anomaly occurence, our initial objective was to make a close scrutiny of craters with specific radar or infrared properties. However, too little of the Moon has been photographed at sufficiently high resolution and low illumination to observe boulders. Therefore, we selected a series of Apollo Panoramic Photographs showing moderate-sized craters (0.5 to 20 km diameter) under sufficiently low lighting to reveal rocky rubble and small pits and then checked the radar and infrared displays to obtain the brightness indices of these craters.

One of us (WKH) made counts of 'boulders' (positive-relief objects about 8–60 m diameter) and pits (mostly 60 to 250 m diameter depressions). The counts were typically made on a suitably-lit sector of the outer rim, about 1.0 to 1.7 radii out from the center. Judging from the appearance of the pits in the crater interiors and rims, as compared with other pits in the surroundings, the small pits were generally identified as primary impact craters and thus believed to be an indicator of the age of the large parent crater being studied. Ages of the large craters were also judged by general morphological properties, such as sharpness of rim presence of rays and floor structures. Thus, it was possible to order the craters in approximate age sequence to study the correlations between age, radar and infrared properties, rock debris densities, and geological background. In this study of Apollo photography, craters were limited to a size range small enough to give a modest statistical sample in a small area, and large enough to allow radar and infrared indentification. Table A-1 gives the craters selected for study. Figure A-1 shows four of the craters selected for study.

There is considerable variability in the number of boulders or blocks thrown out of these small craters. In some areas, such as parts of Mare Serenitatis, many km or sub-km scale craters may have thick clusters of nearby ejected boulders, while in other mare areas, craters which appear morphologically identical have very few ejected boulders. Young *et al.* (1974) report a similar result. Apparently the rock producing mare layers very in depth and coherence. While we have hypothesized that competent rock layers lie much deeper in the megaregolith-covered terrae than in the maria, we do not assume that solid rock layers underlie all maria at a uniform shallow depth. Thus, some scatter in infrared and radar parameters is expected for otherwise similar craters.

Figure 1, the statistics for boulders and pits, supports the conclusion that the presence of ejected boulders (defined here as positive relief protrusions in the size range of 10–60 m, close to the limit of resolution of the available photography) is a strong indicator of relatively young age, and that the number density of boulders declines with increasing age. Figure 1 suggests an inverse relationship between boulder density and pit density. Out of a sample of 19, the six craters with highest boulders density include the five with lowest pit density. Furthermore, Figure A-2 which shows boulder density plotted against the morphological class; indicates that no craters with high boulder

Table A-1

	DIAM. (km)	MORPHOLOGY CLASS[2]	BOULDER DENSITY[2] (DIA. ~ 20 m) km^{-2}	AGE INDEX[3] PITS/km^2 BLDRS/km^2 AT D ≃ 60 m	PIT DENSITY (DIA. 60 m)	10 μm IR CLASS[4]	70 RADAR CLASS[5]	3.8 cm RADAR CLASS[5]	IR-RADAR INDEX
MARE BACKGROUND									
13.5 km SW OF BONPLAND E	0.5	1.0	9.0	0.8	.55	-	-	-	-
PYTHEAS N	3.0	1.8	0.1	130	2.2	FNT	0	0	FFF
GUERICKE E	3.5	1.2	0.9	2.6	.36	FNT	0	0	FFF
TIMOCHARIS E	3.7	1.5	0.7	13	.90	FNT	1.0	1.0	FBB
BONPLAND E	5.7	1.5	0.7	7.0	.85	BRT	0	1.5	FFB
DESEILLIGNY	6.0	?	0.4	20	1.5	BRT	0.5	0	BFF
EUCLIDES D	6.2	1.2	0.5	19	2.1	BRT	0	2.0	BFB
TIMOCHARIS A	6.4	1.6	0.3	32	1.2	BRT	1.0	1.0	BBB
GUERICKE C	10.2	1.3	<0.2	>33	1.6	BRT	-ϕ	2.0	B?B
EUCLIDES C	11.0	1.3	1.2	8.7	1.3	BRT	1.0	2.0	BBB
EUCLIDES B	11.2	1.3	0.4	50	1.7	FNT	2.0	2.0	FBB
EUCLIDES	13.1	1.1	0.4	33	1.9	BRT	2.0	2.5	BBB
PYTHEAS	18.3	1.8	0.45	68	3.0	BRT	3.0	1.0	BBB
TERRA BACKGROUND									
DOLLAND E	5.3	1.1	1.3	6.0	0.8	BRT	0	2.5	BFB
HIPPARCHUS Z	5.8	2.0	<0.1	>240	4.0	FNT	-ϕ	0	F?B
RITCHEY D $\vec{V}$	5.9	1.2	0.3	230	3.7	FNT	2.0	2.0	FBB
SW OF ANDEL M	6.6	3.1	<0.05	>180	1.6	FNT	0	0	FFF
DOLLAND D	8.4	1.5	<0.05	>120	1.2	FNT	0	0	FFF
HIPPARCHUS L	11.6	1.2	<0.3	>200	5.4	FNT	-ϕ	0	F?F
HIPPARCHUS C	18.2	1.0	0.6	47	2.2	BRT	-ϕ	0	B?F

FOOTNOTES:

1. 1 = YOUNGEST, SHARP RIM, FEW OVERLAPPING PITS -- 4 = OLD, BATTERED (ARBITRARILY ASSIGNED).
2. BOULDER COUNTS USUALLY IN AN ANNULUS FROM RIM TO ABOUT 1.7 CRATER RADII.
3. RATIO OF PIT TO BOULDER DENSITIES, CORRELATED WITH APPARENT AGE AND MORPHOLOGY CLASS.
4. BRT = BRIGHT; FNT = FAINT
5. ARBITRARY MEASURE OF STRENGTH OF RADAR RETURN. 0 = NO RETURN
6. TOO NEAR DISK CENTER TO GET RETURN.
7. UPLAND PLAINS BACKGROUND.

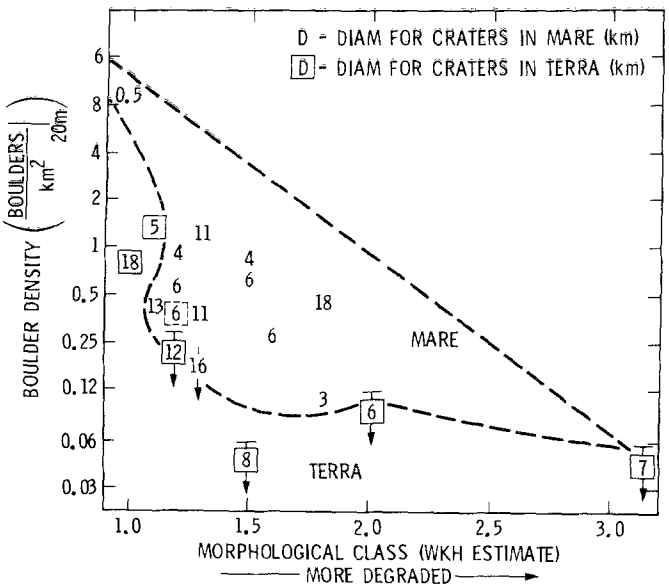

Fig. A-2. Boulder density ('rocks' of diameter about 20 m per km²) versus morphological class, a subjective age criterion based on rim sharpness, floor roughness, ray brightness, etc. Entries are crater diameter (km). Rock density decreased with age, and may tend to be lower for craters in terrae units (boxes) than in for craters in mare units.

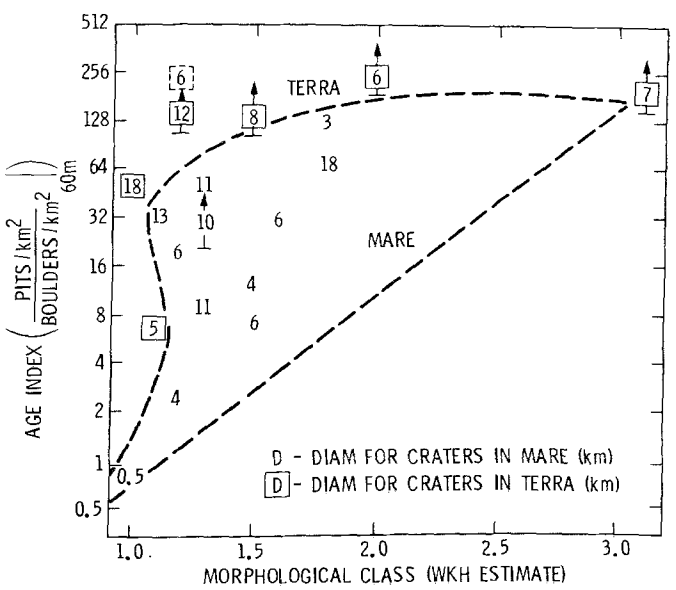

Fig. A-3. Morphological class versus age index, the ratio of pit numbers to rock numbers at diameter around 60 m. This index evidently increases as a function of age. Terra values tend to be higher than mare values for the same morphological class, perhaps due to lower rock densities produced initially in upland craters formed in highly pulverized megaregolith.

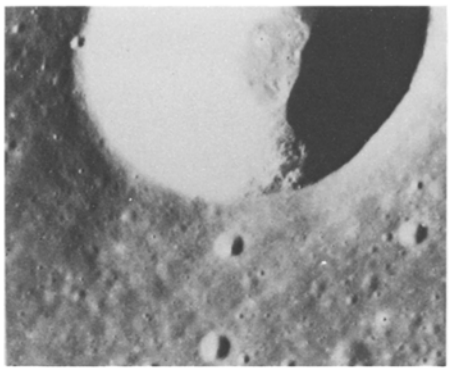

TIMOCHARIS A AS17-3061
6.4 km/MORPH 1.6/MARE/BBB

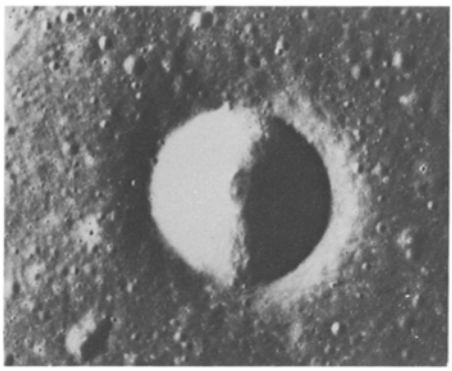

PYTHEAS N AS17-3077
3.0 km/MORPH 1.8/MARE/FFF

RITCHEY D AS16-4578
5.9 km/MORPH 1.2/TERRA/FBB

HIPPARCHUS Z AS16-4578
3.0 km/MORPH 1.8/MARE/FFF

Fig. A-1 Apollo panoramic photographs of four of the eighteen craters studied in detail. See Table A-1.

density were found corresponding to a highly degraded morphological class. Since our study considered only craters with visible boulders, the entire relationship between crater age and boulder density is not given in Figure A-2. There were other craters in the photographs and these craters had no boulders and more degraded morphological age features and larger numbers of overlying craterlets. These craters, which were not included in our study, would have extended both diagrams to the lower right, making the relationships clearer. The implications of Figures 1 and A-2 are that boulders disappear as craters age. This could result from two processes: (1) break up and erosion of boulders by small scale primary and secondary cratering and (2) a slow burial of boulders and boulder fragments by ejecta from nearby craters.

Figure A-2 contains an interesting indication that for a given morphological class, the terra craters have fewer boulders than the mare craters. This is consistent with the hypothesis that the terra consists of a deep megaregolith that contains relatively few rocky fragments. Thus, a crater that penetrates a few hundred meters into this terra mega-

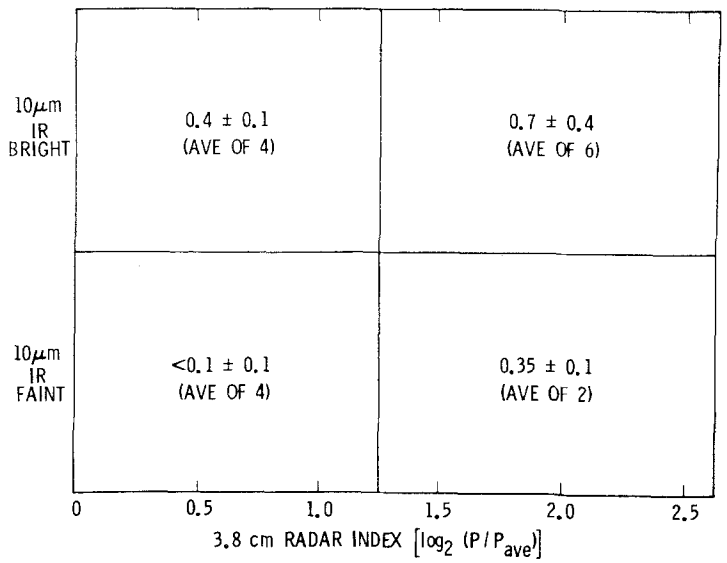

Fig. A-4. Average boulder densities versus 70 cm and 3.8 cm radar indices. Note that craters with bright infrared and high 3.8 echo power have higher boulder densities.

regolith would throw out few competent boulders, while a crater penetrating a similar depth into a mare is much more likely to throw cohesive boulders.

These relations are explored further in Figure A-3 where an age index defined as the ratio between pit density and boulder density is plotted versus morphological class. This ratio is determined at 60 m diameter since the statistics for both pits and boulder frequently overlap at this diameter. This ratio of pits to boulders is believed to be correlated with crater age, since the number of pits increases with age, while the number of boulders declines with age. Figure A-3 also indicates that age index increases with morphological class: since no craters are found in the half of the diagram with low age indices and high morphological classes (as before, this diagram could have been extended to the upper right by including still older craters than those selected here). Again, there is an indication of different behavior for the terra craters and mare craters. For any given morphological class, there is a tendency for the terra craters to have a higher age index, that is, to have a lower ratio of boulders to pits. In other words, if two similar smaller sized craters formed simultaneously, one in mare and one in terra, the terra crater tends to look older when judged by its boulder field, since it is likely to produce fewer boulders. Thus, we suggest that terra craters simply produce fewer boulders originally because of the terra megaregolith is a comminuted material and that boulders in the terra are blanketed more rapidly by nearby impacts than in the mare.

The correlation between these photogeologic properties and the radar properties is not quite as clear, although its interpretation here suffers from a small statistical sample. Previous studies such as Thompson *et al.* (1974) have assumed that a high infrared or radar return involves a high incidence of bare rock or rock fragments such as the boulders

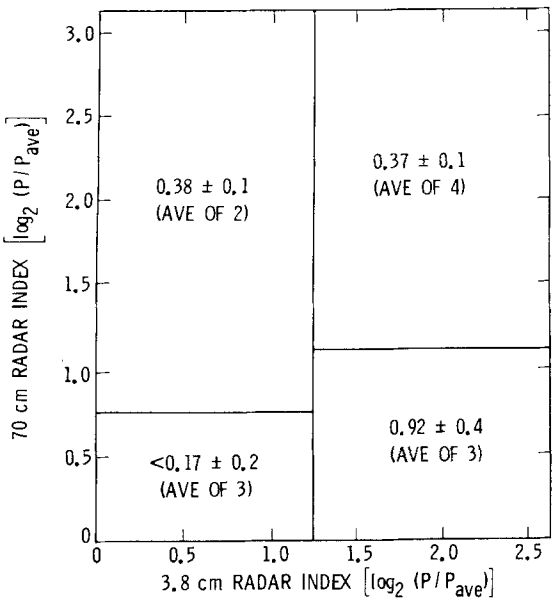

Fig. A-5 Average boulder densities versus 70 cm and 3.8 cm radar indices. Surprising, many craters with high boulder densities have high 3.8 cm radar echoes but low 70 cm radar echoes.

observed here. To study the correlation of surface rocks with infrared and radar anomaly strengths, boulder densitities were averaged for various combinations of infrared and radar anomalies. Figure A-4 shows average boulder densities for different combinations of the infrared 3.8 cm radar signatures. The boulder density from Table A-I was entered for each crater in this field using only craters with diameters between 5 and 19 km (those large enough to be detectable in the infrared data). Because of high scatter among the individual craters, only averages are entered in the four combinations of Figure A-4. These data confirm that older craters without strewn boulder fields do not produce strong infrared and radar signals; conversely, the craters with strong infrared and radar signals are the ones with the highest average boulder densities. A similar relationship is observed when one plots boulder density instead of age index. That is the weakest infrared and radar signatures are associated with high age index craters and the strongest signatures are associated with low age index craters.

Figure A-5 is a plot of average boulder densities versus 3.8 cm and 70 cm echo strengths which shows that the correlations between photogeoligic properties and radar signature are not straightforward. Note that craters with weakest radar signatures have the lowest density of boulders, and this supports our basic hypothesis that boulders correlates with the radar reflectivity. However, the craters with the highest boulder density do not appear to be those with the highest radar reflectivity at both radar wavelengths. Rather, the highest boulder densities are found among craters with high 3.8 cm radar return but low 70 cm radar return. It should be noted that the boulder density referred to here is the density of objects of approximately 20 m diameter and there is no assurance that a high

density of these very large objects necessarily means a high density of rocks whose dimensions are equal to the radar wavelength.

The principal unexpected result in Figures A-4 and A-5. is that that craters with the highest boulder densities are not the ones brightest at 70 cm, but the ones with high 3.8 cm radar response, high infrared emission, but relatively low 70 cm radar response. Two hypotheses for these relationships come to mind. First, our measurement of 20 m boulders may not reveal the radar and infrared sensitive parameters – the density of meter and centimeter sized rocks or the amount of exposed bedrock. Thus, it may be true that high radar and infrared reflectivity always correlates with the presence of small rock or bedrock exposures with dimensions similar to the wavelength. Second, the postulated correlation between exposed rock and infrared and radar brightness may be oversimplified.

The first hypothesis is attrative if fresh craters form ejecta of rocky rubble with steep power-law size distribution, such that radar cross-section is controlled by relatively large numbers of small-sized rocks. It is a characteristic of these size distributions that very small changes in the exponent of the power law can produce large changes in the fraction of the surface area concentrated at either large or small diameters among the fragments (see Hartmann, 1969). The small changes in the exponent are characteristic of different fracturing the grinding histories such as might occur between the ejecta from a partly evolved regolith and a solid rock region. Thus, it is possible that two craters both having fields of 20 m boulders might have different proportions of their radar-reflecting or infrared-emitting rock surfaces concentrated in different size areas or different types of units of bedrock. Thompson *et al.* (1974) also noted that craters with large 3.8 cm radar echoes often had little or no 70 cm enhancement and a definite thermal anomaly. These findings suggest that further study of the differences between the infrared 3.8 cm radar, 70 cm radar, and photographically detectible boulder characteristics could further elucidate the characteristics of the lunar subsurface in different regions.

In summary , this study of Apollo panoramic photographs yields the following results. (1) Young craters appear to be rocky and the density of rocky rubble on the crater rims appears to decrease with the increasing age of the craters. (2) Old craters, which have little or no visible boulder ejecta in the diameter range 10–160 m, have very weak infrared and radar signatures. (3) Craters that do have dense fields of boulders in the 10–60 m diameter range often tend to have high 10 μm infrared and 3.8 cm radar signatures, but weaker 70 cm radar signatures. (4) Finally, among the 3 to 18 km diameter craters studied here, fewer blocks may have formed initially (or they may disappear faster) for terra craters than for mare craters.

Appendix B. Systematic Errors in Identification of Blocky Craters from Infrared and Radar Anomalies

This appendix addresses the possibilities for systematic errors in the identification of blocky craters from infrared and radar anomalies. First, there is the possibility that smaller blocky craters with sizes comparible to the resolution of the infrared and 70 cm

radar observations may be misidentified as being average. In addition, two other possible errors depend upon crater position with respect to limb. The infrared resolution is coarser toward the limb, which would cause smaller blocky craters to be misidentified as not being anomalous; radar echoes are strongly modulated by slopes for craters toward the limb and this might cause some craters to have strong echoes which are not associated with rocks. To study these possible errors in detail, the infrared and radar anomaly statistics for the Middle and Outer Ring areas shown in Figure 2 were compared with each other.

Let us now examine these errors in greater detail. The two errors which could cause Middle Ring–Outer Ring differences are as follows. First, a systematic enlargement of the infrared resolution cell-size toward the limb which would cause some small blocky craters to be misidentified as not being infrared anomalies. One notes that the infrared resolution cell size, which was 14.5 km at the center of the disk, varies between 17 and 19 km for the Middle Ring and between 21 and 28 km for the Outer Ring. Second, possible misidentifications of rim echoes as blocky floor echoes for small craters toward the limb would tend to raise the radar anomaly counts for the Outer Ring over the Middle Ring. This effect arises since the depolarized radar echoes have an average behavior proportional to $\cos(\theta)$, where θ is the angle of incidence. Thus, radar enhancements from slopes are smaller toward the center of the disk and larger toward the limb. However, strong rim echoes require steep rim slopes, which occur only on the youngest craters. These youngest craters in both mare and terra will be blocky anyway.

Another possible error source is the loss of infrared and radar strength for craters that are smaller than resolution cells. Thus, a small crater may be blocky but not large enough to generate a visible anomaly. This effect would cause some small blocky craters to be identified as infrared of 70 cm 'faint'. This error depends upon crater size only for the 70 cm radar and depends upon the crater's position with respect to the limb for the infrared anomalies. For brevity, we will use the term 'resolution confusion' for the apparent loss of infrared and 70 cm radar anomaly indications for craters smaller than their respective resolution cell size. We expect no 3.8 cm radar 'resolution confusion' effects since the 3.8 cm radar cell size of 1–3 km is smaller than lower limit of 4 km for our plots.

To examine the effect of these possible errors on the data, crater-size distributions of the more common anomaly types (BBB, FBF, FBB, and FFB) were plotted for the Middle and Outer Areas of Figure 2. The comparison of the BBB (bright infrared, 3.8 cm and 70 cm radar) anomalies in the Mddle and Outer Rings showed that there were only 3.2% more mare craters with diameters less than 20 km in the Middle Ring than in the Outer Ring; terra craters statistics in the two rings were nearly identical. The small difference in mare craters was attributed to infrared and 70 cm radar resolution confusion since some smaller blocky craters which are actually BBB type craters appear as FBB of FBF type craters. There is no evidence that radar crater rim effects are artifically raising Outer Ring counts. Also, the differences between the two rings was small enough that the data from the Middle and Outer Rings was combined to give the differential and cumulative crater distributions shown in Figure 3.

The Middle and Outer Ring plots for the FBB (faint infrared, bright 3.8 cm and 70 cm radar) anomalies showed that both mare and terra craters with diameters smaller than 20 km were 50% more frequent in the Middle Ring than in the Outer Ring. This is opposite to the effects predicted by infrared resolution confusions, since the Outer Ring should have more FBB type craters which would have appeared as BBB type craters had the infrared resolution been better. The observed difference is also opposite to that predicted for radar crater rim effects. However, the differences are small enough that the data for the two rings were combined, giving the differential and commulative distributions for the FBB anomaly type are shown in Figure 4(a).

The Middle Ring and Outer Ring Plots for the FBF (faint IR, bright 3.8 cm, faint 70 cm radar) anomalies had nearly equal densities of small craters in the Middle and Outer Ring. Here, the density of small mare craters with diameters less than 20 km were identical while terra craters with diameters less than 20 km were 15% more frequent in the Middle Ring than the Outer Ring. Unlike the FBB anomalies, the observed differences is that predicated for infrared resolution confusion and for radar crater-rim effects. As before, the difference between the Middle and Outer Rings is small enough, that the data were combined and cumulative and differential crater distributions for the FBF anomaly types are shown in Figure 4(b).

Unlike the BBB, FBB, and FBF types, the FFB (faint IR and 3.8 cm radar, bright 70 cm radar) anomaly type had significant differences between the Middle and Outer Rings. In particular, the total number of terra craters in the Middle Ring is 2.5 times the number of terra craters in the Outer Ring. We have no explanation for this effect. A systematic error is unlikely since there was good agreement between Middle and Outer Rings for the other anomaly types; and we know of no physical effect which would give this result. However, given this discrepancy, the Middle and Outer Ring statistics are plotted separately in Figure 5.

A comparison of the differential plots for the BBB, FBB, and FBF craters provides an insight into errors from resolution confusion. The differential plot of the BBB anomaly (Figure 3) shows a drop at crater diamters near 8 km which we attribute to resolution confusion of the infrared anomalies. The craters disappearing from the BBB differential plots should appear elsewhere. Note that the differential plot for the mare FBB anomalies shows a peak near crater diameters of 7 km, the probable result of falsely counting BBB type craters as FBB type craters. These differential plots of FBB anomalies also show a drop at crater diameters near 5 km, the probable result of resolution confusion in the 70 cm radar images. Similarly, the number of mare FBF type craters tend to rise as the FBB type craters tend to decrease near diameters of 5 km. This is expected result of miscounting FBB type craters as FBF type craters because 70 cm radar enhancement are not observed because of resolution confusion.

In summary, we feel that there is no significant center-to-limb effects except for the unexplained difference in terra FFB craters for the Middle and Outer Rings and the various problems which caused us to reject the Central Area. Resolution confusion, the loss of signatures when craters are smaller than resolution elements, is a significant factor.

References

Aggarwal, H. R. and Oberbeck, V. R.: 1979, Abstract, *Tenth Lunar and Planetary Science Conference*, Houston, Texas, 6–9.

Arthur, D. W. G. *et al.*: 1963, *Communications of the Lunar and Planetary Laboratory* 2, 71.

Arthur, D. W. G. *et al.*: 1964, *Communications of the Lunar and Planetary Laboratory* 3, 1.

Arthur, D. W. G. *et al.*: 1965, *Communications of the Lunar and Planetary Laboratory* 3, 61.

Arthur, D. W. G. *et al.*: 1966, *Communications of the Lunar and Planetary Laboratory* 5, 1.

DeHon, R. A.: 1973, *Proc. 5th Lunar Science Conf.* 53.

DeHon, R. A.: 1978, *Proc. 9th Lunar Science Conf.* 633.

Gold, T.: 1977, *Phil. Trans. R. Soc., London A* 285, 555.

Hartmann, W. K.: 1969, *Icarus* 10, 201.

Hartmann, W. K.: 1973, *Icarus* 18, 634.

Hörz, F. *et al.*: 1976, *Proc. 7th Lunar Science Conf.* 2911.

Kavack, R. L. and Watkins, J. S.: 1973, *The Moon* 7, 63.

McGetchin, T. R., Settle, M. and Head, J. W.: 1973, *Earth Planet. Sci. Lett.* 20, 266.

Moore, H. J., Hodges, C. A. and Scott, D. H.: 1974, *Proc. 6th Lunar Sci. Conf.* 71.

Peeples, W. J. *et al.*: 1978, *J. Geophy. Res.* 83, 3459.

Phillips, R. J. *et al.*: 1972 *J. Geophys. Res.* 77, 7106.

Pike, R. J.: 1977, Size Dependence in the Shape of Fresh Impact Craters on the Moon, in D. J. Roddy, R. O. Pepin and R. B. Merrill (eds.) *Impact and Explosion Cratering* Pergamon Press, New York, 489–509.

Ronca, L. B.: 1970, *The Moon* 2, 202.

Shoemaker, E. M. *et al.*: 1970, *Proc. Apollo Lunar Sci. Conf.* 2399.

Short, N. M. and Forman, M. L.: 1972, *Modern Geology* 3, 69.

Shorthill, R. W.: 1973, *The Moon* 7, 22.

Thompson, T. W.: 1974, *The Moon*, 10, 51.

Thompson, T. W., Masursky, H., Shorthill, R. W., Tyler, G. L. and Zisk, S. H.: 1974, *The Moon* 10, 87.

Thompson, T. W., Moore, H. J., Schaber, G. G., Shorthill, R. W., Whitaker, W. E. and Zisk, S. H., Final Report: *Apollo Experiment S-217, IR/Radar Study of Apollo Data,* JPL Technical Memorandum 33–787, Jet Propulsion Laboratory Pasadena, Calif., 1 Oct. 1976.

Woronow, A. *et al.*: 1978, *Standard Techniques for Presentation and Analysis of Crater Size-Frequency Data,* NASA TM 779730. (also published in *Icarus* 37, 29 (1979)).

Young, R. A. *et al.*: 1974, *Proc. 6th Lunar Science Conf.* 153.

Zisk, S. H. and Moore, H. J.: 1972, Calibration of Radar Data from Apollo 16 Results, Part X of Photogeology, in *Apollo 16 Preliminary Science Report,* NASA SP-315, pp. 29-110 to 29-113. National Aeronautics and Space Administration, Washington, D.C..

Zisk, S. H., Pettengill, G. H., and Catuna, G. W.: 1974, *The Moon* 10, 17.